Published online 20 September 2016 *Nucleic Acids Research, 2016, Vol. 44, No. 21* ***10467–10479***
doi: 10.1093/nar/gkw846

Dynamic peptides of human TPP1 fulfill diverse functions in telomere maintenance

Malligarjunan Rajavel[1], Tivadar Orban[1], Mengyuan Xu[1], Wilnelly Hernandez-Sanchez[1], Maria de la Fuente[1], Krzysztof Palczewski[1] and Derek J. Taylor[1,2,*]

[1]Department of Pharmacology, Case Western Reserve University, School of Medicine, Cleveland, OH 44106, USA and [2]Department of Biochemistry, Case Western Reserve University, School of Medicine, Cleveland, OH 44106, USA

Received May 04, 2016; Revised September 12, 2016; Accepted September 14, 2016

ABSTRACT

Telomeres are specialized nucleoprotein complexes that comprise the ends of linear chromosomes. Human telomeres end in a short, single-stranded DNA (ssDNA) overhang that is recognized and bound by two telomere proteins, POT1 and TPP1. Whereas POT1 binds directly to telomere ssDNA, its interaction with TPP1 is essential for localization of POT1 to the telomere. TPP1 also provides enhanced binding and sequence discrimination that regulates POT1-TPP1 interactions exclusively with telomere ssDNA. Finally, TPP1 recruits telomerase, the enzyme responsible for synthesis of telomere DNA, to the telomere. While the oligosaccharide–oligonucleotide-binding (OB)-fold domain of TPP1 has been solved by X-ray crystallography, the molecular interactions within the POT1-TPP1-ssDNA ternary complex and the conformational changes that contribute to its diverse functions remain ambiguous. We employed hydrogen/deuterium exchange combined with mass spectrometry to identify three peptides, all residing within the OB-fold of TPP1, that exhibit altered exchange rates upon complex formation or ssDNA binding. Mutation of these regions combined with functional assays revealed the diverse contributions of each moiety in protein–protein interactions, regulating telomerase activity or DNA-binding. Together, these functional data combined with biophysical analyses and homology modeling provide a molecular understanding of the diverse contributions of TPP1 in telomere maintenance.

INTRODUCTION

Telomeres are specialized nucleoprotein complexes residing at the ends of all linear chromosomes that maintain proper genome stability and prevent the activation of illicit DNA damage response signaling pathways (1–3). Telomere DNA is composed of repeating G/T-rich tracts, which extend for thousands of bases before ending in a single-stranded DNA (ssDNA) overhang at the 3′ end that is 50–200 nucleotides long in humans (4–6). A set of specialized telomere-end binding proteins constitutes the shelterin complex, which is responsible for recognition and protection of telomere DNA (7). Within shelterin, Telomeric Repeat-binding Factors (TRF1 and TRF2) recognize double-stranded telomere DNA (dsDNA) (8,9), and the Protection of Telomere 1 (POT1) protein binds to the ssDNA overhang (10). Other telomere proteins, including TRF interacting protein (TIN2), Repressor/Activator Protein 1 homolog (RAP1) and TPP1 (formerly known as PIP1, PTOP and TINT1) interact with TRF1, TRF2 and POT1 to shield telomere DNA and protect it from damage (7,11–19). The shelterin proteins are also key players in both positively and negatively regulating the activity of telomerase, a specialized reverse transcriptase that synthesizes and extends telomere DNA (18,20–23).

TPP1 is arguably the most versatile of the shelterin proteins, as it contributes to several diverse roles in maintaining telomere length and integrity. By interacting with TIN2 and POT1, TPP1 forms an intimate connection within the shelterin complex, thereby bridging the dsDNA and ssDNA components and assisting in the localization of POT1 at the telomere (14,17,24–26). By forming a heterodimer with POT1, TPP1 increases the affinity of POT1–TPP1 for ssDNA over that of POT1 alone and aids in the selectivity of ssDNA over RNA substrates (18,23,27). Furthermore, TPP1 actively recruits telomerase to the telomere and functions as a telomerase processivity factor when coupled with the POT1 protein (18,23,28,29). Finally, when combined with POT1, TPP1 aids in disrupting secondary structures, including G-quadruplexes that are intrinsic to G-rich telomere DNA (30–32) and restricts telomere resection after DNA replication (33,34). Despite an appreciable amount of data focused on TPP1 function, however, it remains unclear as to how this protein can regulate so many different

*To whom correspondence should be addressed. Tel: +1 216 368 0684; Fax: +1 216 368 1300; Email: derek.taylor@case.edu

processes and what molecular alterations govern the switch from one action to another.

TPP1 is a multi-domain protein that includes an N-terminal oligosaccharide–oligonucleotide-binding (OB)-fold domain, a POT1 binding domain (PBD) and a C-terminal TIN2-interacting region (23,24). The TPP1 OB-fold domain reveals a conserved structural scaffold comprised of ∼160 residues organized into a β-barrel of five strands and capped with a C-terminal α-helix (23). As the name implies, OB-fold motifs are commonly involved in mediating protein-nucleic acid interactions. Some ssDNA-binding proteins with at least one OB-fold domain include human POT1, RPA (replication protein A), breast cancer 2 (BRCA2) early onset proteins, Stn1-Ten1 proteins in *Saccharomyces cerevisiae*, *Schizosaccharomyces pombe* and human, *S. cerevisiae* Est3 and *Sterkiella nova* TEBPα and TEBPβ proteins (16,35–39). Despite sharing little sequence identity, the structures of OB-fold containing proteins solved by x-ray crystallography feature remarkable structural conservation. While the β-barrel within the OB-fold architecture is similar in all these structures, the peripheral peptides that connect the individual β-strands display the greatest structural variability (40). Since the universal OB-fold architecture is used to bind substrates with a range of primary sequences, the specificity for a particular DNA ligand likely arises from differences in the peripheral loops and their respective conformations (41,42).

Hydrogen–deuterium exchange (H/DX) combined with mass spectrometry (MS) is an established and powerful tool used to understand the structural and dynamic aspects of proteins and complexes in solution (43–46). This method relies on the fact that exposure of a hydrated protein or complex to D_2O induces amide hydrogen exchange for deuterium. As such, H/DX functions as a reporter for analyzing local structures as the exchange rate is affected by factors that include solvent accessibility of individual peptides as well as inter- and intramolecular interactions that affect the dynamics, accessibility and/or stability of the peptide fragment. After exposure to deuterium, proteolysis is coupled with MS-based peptide mapping to measure the deuteration of individual protein peptide fragments through extremely sensitive mass shifts. Here, we used H/DX coupled with MS to identify the conformational dynamics for different areas of the human TPP1 protein. Our data pinpoint regions of TPP1 that displayed altered degrees of hydrogen–deuterium exchange upon POT1 binding and also for binding of the POT1–TPP1 complex to telomere ssDNA. The most significant changes in H/DX of TPP1 occurred in three regions, all residing within the peripheral regions of the OB-fold domain. We demonstrate the importance of these segments in protein–protein interactions, in DNA binding and in telomerase-mediated primer extension. In summary, our data provide insights into the dynamics of TPP1 while deciphering the functional details of its distinct and diverse roles at a molecular level.

MATERIALS AND METHODS

Protein expression and purification

For H/DX studies, an N-terminal 6 × His-tagged TPP1 construct comprising the POT1- and telomerase interaction domains was expressed either alone or together by co-expression with full-length POT1 protein using the recombinant baculovirus expression system to infect *Spodoptera frugiperda* 9 (Sf9) insect cells as described previously (47,48). Cells were pelleted 24–72 h post-infection and suspended in lysis buffer containing 25 mM HEPES pH 8.0, 150 mM NaCl, 5 mM DTT, 5 mM benzamidine, 1 mM phenylmethylsulfonyl fluoride and 1 complete ULTRA protease inhibitor cocktail tablet (Roche Diagnostics, Indianapolis, IN, USA). For functional assays, GST-POT1 was expressed with recombinant baculovirus and Sf9 cells as described above and the TPP1 construct (wild-type and mutants) was expressed in *Escherichia coli* BL21 (DE3) cells as a fusion protein with an N-terminal 6 × His-tag. *E. coli* were grown at 37°C in lysogeny broth to an O.D. 600 (optical density at 600 nm) of ∼0.6 and then induced with 1 mM isopropyl β-D-1-thiogalactopyranoside. After induction, temperatures were reduced to 20°C and bacteria were grown overnight.

Cells were lysed by sonication and then incubated with RQI DNase (Promega, Madison, WI, USA) for 30 min before pelleting cellular debris by ultracentrifugation at 150K × *g* for 45 min. Following ultracentrifugation, the supernatant of 6 × His-tagged proteins/complexes was applied to a gravity filtration column with buffer washed high-density nickel cross-linked beads (Gold Biotechnology, St. Louis, MO, USA). Bead binding was carried out at 4°C, and then beads were rinsed with protein buffer containing 25 mM HEPES pH 8.0 and 150 mM NaCl. Beads were subsequently washed with protein buffer containing 20 mM imidazole before the protein was eluted with protein buffer containing 200 mM imidazole. A total of 6 × His-TPP1 grown in *E. coli* were subjected to anion exchange chromatography with a Hi-Trap-Mono Q column (GE Healthcare). GST-POT1 was purified by binding to a glutathione agarose resin (Gold Biotechnology, St. Louis, MO, USA), rinsed in protein buffer and then eluted with 15 mM glutathione in protein buffer, as previously described (16). The GST-tag was removed by digestion with PreScission Protease (GE Healthcare) as previously described (16,48,49). All proteins were further purified by size-exclusion chromatography over a Superdex 200 HiLoad 16/60 column (GE Healthcare) on an AKTA Purifier 10 system (GE Healthcare). Protein fractions were pooled, concentrated with a Millipore Amicon Ultra 10K centrifugal column, flash-frozen and stored at −80°C.

Hydrogen/deuterium exchange

H/DX experiments were conducted with 10 μg of protein for each experiment. Purified TPP1 protein was diluted in 80% D_20 and steady-state exchange rates were determined at multiple time points ranging from 0 to 20 min. After quenching and pepsin digestion, the percent of deuterium uptake for individual peptides was plotted against time. This evaluation demonstrated that steady-state exchange rates were achieved after 10 min under these conditions (Supplementary Figure S1). These data are in agreement with the optimal D_2O exposure time to achieve steady-state exchange conditions for other peptides interrogated by similar experimental procedures (45,50–52). Therefore, protein

samples were diluted in 80% D_2O and incubated on ice for 10 min.

The exchange was terminated by the addition of 10 μl of quenching buffer (ice cold formic acid, pH 2.5) kept on ice. After the hydrogen–deuterium exchange process was quenched, 10 μl of pepsin (1.7 mg/ml; Worthington, Lakewood, NJ, USA) was immediately added to the solution and the digestion time was set to 10 min on ice. Next, the proteolysed sample was loaded onto a Luna 20 × 2.00 mm C18 column (Phenomenex, Torrance, CA, USA) with the temperature of the Hewlett-Packard autosampler set to 4°C and the high pressure (or high performance) liquid chromatography (HPLC) column kept submerged in ice during the run to minimize back-exchange. Peptides were eluted with the following gradient sequence: 0–4 min, 98% H_2O with 0.1% (v/v) formic acid (A) and 2% acetonitrile with 0.1% (v/v) formic acid (B); 4–12 min, 98–2% A. Separation was performed with an Agilent 1100 HPLC system (Agilent Technologies, Santa Clara, CA, USA) at a flow rate of 0.2 ml/min. The HPLC apparatus was coupled to a Thermo Finnigan LXQ (Thermo Scientific, Waltham, MA, USA) mass spectrometer. Fragments of the peptic digest in the eluent were directed to an electrospray ionization source operated in the positive ion mode. The mass spectrometer was tuned with a standard peptide as previously described (50). The activation type was set to collision-induced dissociation, normalized collision energy to 35 kV, capillary temperature to 370°C, source voltage to 5 kV, capillary voltage to 43 V, the tube lens to 105 V and mass spectrometry spectra were collected over a 200–2000 Da m/z range.

After each HPLC run, a mock injection of 10 μl of mqH_2O was performed to ensure that all peptides were eluted before the next run was conducted. All mock runs were accomplished by the same HPLC methods described for the production runs. Each time, the column was equilibrated for the next production run by using a regimen that consisted of 98% A and 2% B for 20 min with a flow rate set to 0.2 ml/min. All experiments were performed in triplicate.

Analysis of peptide fragments and quantification of H/DX

Peptic fragments were identified through a targeted database search that employed the freely available MassMatrix software (53,54). The database was constructed from the primary sequence of the protein under study. The search criteria used to identify the fragments resulting from the peptic digest were as follows: the precursor ion tolerance was set to 0.8 Da, the maximum number of variable modifications allowed for each peptide sequence was set to 2, the minimum peptide length was set to 4 amino acids, the minimum pp score was set to 5, the pp_{tag} (53) score was set to 1.3, the maximum number of combinations of different modification sites for a peptide match with modifications was set to 1, and the maximum number of candidate peptide matches for each spectrum output in the result was set to 1. The product ion tolerance was set to 0.8 Da, and the mass type was set to average. Statistical significance of the identified peptides was evaluated based on scoring described elsewhere (53,54). An example of peptide validation, including statistical analysis, carried out in this way is presented in Supplementary Figure S2.

Peptides that were reproducibly identified are illustrated in Figure 1. Raw data in the form of relative signal intensity (%) as a function of m/z were extracted with XCalibur 2.1.0. Qual Browser was used for semi-automated peak detection and the deconvolution procedure was performed with HD-Express software (55). Briefly, after deuterium uptake was evaluated in the raw data, the value for every peptide fragment was normalized to 80% of the theoretically maximum exchangeable sites to account for the 80% deuteration (Figure 1). Only peptide bonds were used to account for the amide exchange; deuterium exchange from side chains was considered negligible and was not included in our calculations. The number of exchangeable sites was reduced by the number of proline residues present in the peptic fragments. Graphical and statistical analyses were carried out with Origin 8 SR0 software (version 8.0725, OriginLab Corporation, Northampton, MA, USA). Peptide fragments that were identified in all three samples (18 peptide fragments) represented 93% sequence coverage for TPP1 in all 3 states (TPP1-alone, POT1–TPP1 and POT1–TPP1–ssDNA) (Figure 1, Supplementary Figure S3). Error bars represent standard deviations. Deuterium uptake is shown as values normalized to the theoretical maximum of exchangeable sites within each peptide fragment.

Circular dichroism spectroscopy

Circular dichroism (CD) spectra were obtained with an Applied Photophysics π*-180 spectrometer (Applied Photophysics Ltd, UK). A quartz cell cuvette (Hellma USA Inc., Plainview, NY, USA) with a 2 mm path length was used to acquire CD spectra from 200–280 nm with a 1-nm bandwidth, 2-nm step size and 2-s collection time per data point. Prior to the experiment, the protein samples TPP1-(WT, L_{23}, L_{45} and P1) were thawed in ice and diluted to 5 μM from stock (∼2 mg/ml concentration) in 5 mM HEPES, pH 8.0 and 75 mM NaCl. Protein concentrations were estimated on the basis of UV-absorbance readings obtained with a NanoDrop spectrometer (Thermo Fisher Scientific, Inc., Waltham, MA, USA). The TPP1-WT (denatured) sample was treated with 8M urea and heat-denatured at 95°C for 10 min followed by slow-cooling to 20°C. All spectra were plotted after applying the proper buffer corrections. The mean residue ellipticity was calculated from the observed ellipticity values and protein concentrations, and plotted against the standard wavelengths from 200 to 280 nm (Supplementary Figure S4).

GST–POT1–TPP1 pulldown assay

Purified GST-tagged-POT1 was used at a fixed concentration of 10 nM and incubated with increasing concentrations (∼4 nM to 1 μM) of His-tagged-TPP1-WT and Glutathione Sepharose 4B beads (GE Healthcare) in a binding buffer (25 mM HEPES pH 7.4, 150 mM NaCl, 0.2% NP-40) for 2 h at 4°C. After thorough washing, the beads were collected and heated to 95°C in loading buffer (300 mM Tris-HCl pH 8.0, 10% SDS, 20 mM EDTA, 25% β-mercaptoethanol, 0.1% bromophenol blue, 50% glycerol) to release bound proteins, which then were analyzed by SDS-PAGE. The 'input' controls indicate the immunoblot of

each protein component before incubation. For His-TPP1, input was 2.5% of the highest concentration (1 μM) and 10% for GST and GST-POT1 (10 nM). After SDS-PAGE separations for 1 h at 180 V, samples were transferred to nitrocellulose membranes that were then blotted with anti-6X His antibody (Sigma) and anti-GST antibody (Sigma). Infrared-labeled secondary antibody (LI-COR) was used to produce infrared signals that were developed with the Odyssey Infrared Imaging System. Purified GST-tagged-POT1 at 10 nM was incubated with 500 nM TPP1 (WT or mutant) and detected following the protocol described above.

Filter-binding assay

Filter-binding experiments were carried out for POT1 alone and for POT1–TPP1–(WT, L_{23} and L_{45}) complexes by incubating protein concentrations ranging from 0.6 nM to 360 nM with a constant concentration (0.5 nM) of γ-^{32}P labeled telomeric ssDNA (hT12wt). Prior to this reaction, proteins were diluted to a fixed 8 μM concentration in a protein buffer containing 60 mM HEPES pH 8.0, 75 mM NaCl and 10 μg/ml BSA. Telomeric DNA was diluted in a buffer containing 60 mM HEPES, pH 8.0, 75 mM NaCl and 0.1 mg/ml of tRNA. The filter-binding apparatus was assembled with a precooled nitrocellulose membrane (Whatman), a positively charged nylon membrane (Hybond N^+, GE) and filter paper (Whatman), all fixed in a 72 well slot-blot apparatus. Reaction mixtures were incubated on ice for 30 min, and then the solution was passed through the filter-binding apparatus under vacuum and rinsed once with an equivalent volume of cold buffer. The membranes were air-dried and exposed on a phosphorimager cassette for ∼1 h for freshly labeled DNA. Radioactivity was then quantified using a Typhoon FLA 9500 biomolecular imager (GE Healthcare) and densitometry was performed using ImageQuant TL 1D v8.1 software (GE Healthcare). Fitted curves were calculated for each trial and the reported values represent the average, with calculated standard deviations, derived from three independent experiments for every condition.

Direct telomerase incorporation assay

Telomerase activity assays were performed by mixing 2 μl of hTR and hTERT transfected HEK 293T cell lysate into a 16 μl reaction mixture containing: 35 mM Tris-HCl, pH 8.0, 0.7 mM $MgCl_2$, 1.8 mM β-mercaptoethanol, 0.7 mM spermidine, 35 mM NaCl, 500 μM dTTP, 500 μM dATP, 2.9 μM dGTP, 2 μl [α-^{32}P]-dGTP (10 μCi/μl, 3000 Ci/mmol, Perkin–Elmer) and 1 μM 18-nt substrate $d(GGGTTA)_3$ primer. Purified POT1–TPP1–(WT, L_{23} and L_{45}) protein complexes were added to a final concentration of 1 μM in 150 mM NaCl and 25 mM HEPES, pH 8.0. For those reactions without POT1–TPP1 protein, an equivalent volume of the appropriate (NaCl) protein buffer was used instead. The telomerase reaction was carried out for 30 min at 30°C and then quenched by adding 100 μl of 3.6 M NH_4OAc, 20 μg of glycogen, 4 μl of 10 mM EDTA and a 5′-^{32}P-labeled hT18 primer $(GGGTTA)_3$ as a loading control. The radioactivity of the loading control was determined by liquid scintillation counting and 400 cpm were loaded into each reaction mixture. All ssDNA products synthesized in the assay were ethanol-precipitated and then analyzed on a 12% polyacrylamide/7 M urea/1X TBE denaturing gel. After the run, the gel was dried and subjected to densitometry results of which were detected with a Typhoon Trio PhosphorImager (GE Healthcare) and quantified by ImageQuant TL 1D v8.1 software (GE Healthcare).

Quantification of telomerase assay products was performed as described previously (29,49). Briefly, relative intensities for each hexamer repeat were determined and normalized against the loading control for each lane. Total activity is reported as total lane counts by summing the relative intensities of all normalized bands within a lane. Repeat addition processivity was calculated by first correcting for the number of radiolabeled Gs incorporated within each hexamer repeat and then calculating the fraction left behind (FLB) by subtracting and dividing the sum of intensities for each round of extension (1-*n*) by the entire sum of intensities for the total lane count. The ln (1-FLB) was plotted against the repeat number of telomerase extension and the slope was fitted to the linear portion of those data, which are represented as repeat round numbers 5–20 in the telomerase assay. Repeat addition processivity was defined as $-0.693/\text{slope}$.

RESULTS

H/DX-MS analysis of TPP1 reveals regions of altered solvent exchange that are dependent on complex formation

We employed H/DX-MS to identify dynamic regions and/or structural rearrangements in TPP1 that occur in response to binding of POT1 or POT1–ssDNA. Experiments were performed with purified full-length POT1 protein and a well-characterized, truncated version of TPP1 (representing amino acids 89–334), that maintains both its POT1-binding and telomerase-enhancement properties (18,23,29,31,47–49,56,57). For these experiments, TPP1 protein was expressed and purified as either an individual protein or in complex with POT1 as a POT1–TPP1 heterodimer. The POT1–TPP1–ssDNA complex was prepared by incubating hT12wt ssDNA with the POT1–TPP1 complex followed by gel filtration chromatography to isolate this complex. Analysis of TPP1 peptides over time revealed that H/DX reaches a steady-state exchange after 10 min when diluted from H_2O into an 80% D_2O solution (Supplementary Figure S1). This behavior is comparable to what is observed for many peptides investigated under similar conditions (45,50–52). Accordingly, TPP1 protein and complexes were subjected to hydrogen–deuterium exchange for a period of 10 min, at which point H/DX was quenched by acidification.

Following exposure to deuterium and subsequent pepsin digestion, peptide fragments were analyzed using liquid chromatography-electrospray ionization-tandem mass spectrometry. Peptic peptides were identified using collision-induced dissociation followed by comparison to the theoretical peptide *y* and *b* fragments. Peptides were selected with a statistical approach described in *MassMatrix* (58). Because of differences in peptide properties (e.g. different retention time, represented abundance, different sequence and secondary structure, etc.), we only compared

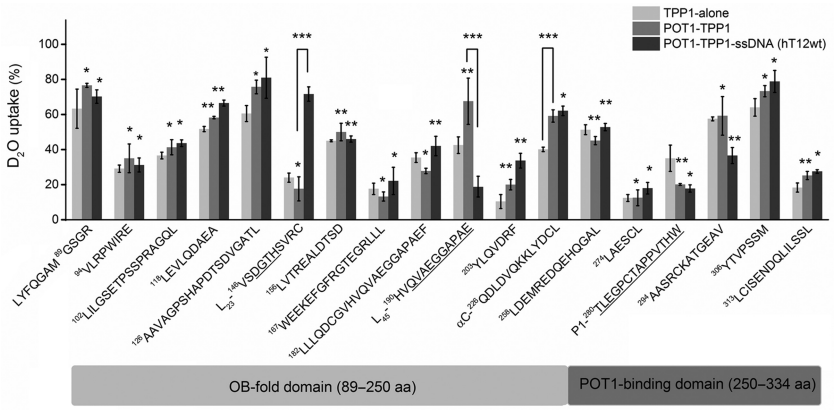

Figure 1. Changes in H/DX of TPP1 upon POT1 and ssDNA-binding. Data bars represent the percent of deuterium uptake (from the D_2O solvent) for individual peptide fragments of TPP1 in three states: TPP1-alone, POT1–TPP1 complex and POT1–TPP1–ssDNA complex. Tukey's multiple comparison test was used to compare deuteration between the three states, with significant differences labeled. The *P*-values were classified and defined as $P > 0.05$ (*); $0.05 > P > 0.001$ (**) and $P \leq 0.001$ (***). Three peptide fragments within the TPP1 OB-fold demonstrated notable variations ($P = 0.001$–0.0001) in at least one of the conformational states. These peptides are labeled as L_{23}, L_{45} and αC, according to their secondary structure (loop or helix) in the overall structure solved by X-ray crystallography. An additional peptide residing within the known POT1-binding domain was labeled P1 and further analyzed. All peptides were identified based on their retention times in HPLC elution and ionization states. The percentage of deuteration was recorded based on the m/z shifts in comparison to the hydrated (non-deuterated) states. All experiments were performed in triplicate with errors (SEM) shown.

deuterium uptake for identical peptides that were identified for TPP1 in all three states (TPP1-alone, POT1–TPP1 and POT1–TPP1–ssDNA) (Figure 1, Supplementary Figure S3). These results indicated only modest changes in deuterium uptake for most of the TPP1 peptic fragments within the three samples (Figure 1, Supplementary Figure S3). However, three peptides, all within the OB-fold domain of TPP1, displayed significant changes in H/DX that could be attributed to the presence of POT1 and/or ssDNA (Figure 1, Supplementary Figure S3). The first peptide, designated L_{23}, represents amino acids V146-C155 in the primary sequence. This region demonstrated relatively little difference in H/DX upon comparing free TPP1 with the POT1–TPP1 heterodimer. Addition of ssDNA to the POT1–TPP1 complex, however, resulted in a significant increase in deuterium exchange for the L_{23} peptide in the TPP1 protein. Another peptide, also within the OB-fold domain (L_{45}; amino acids H190-E201), showed a slight, yet statistically significant increase in H/DX upon POT1-binding coupled with a significant decrease in H/D exchange when ssDNA was bound to the POT1-TPP1 complex (Figure 1). The final peptide is part of the C-terminal helix region of the TPP1 OB-fold (αC; amino acids Q226-L238). This fragment displayed a significant increase in H/DX upon POT1-binding, and with no additional changes upon ssDNA binding (Figure 1).

Probing the functional roles of identified TPP1 peptides

Our H/DX experiments identified TPP1 peptides with altered rates of solvent exchange as a function of POT1- or POT1–ssDNA complex formation. Based on these data, and additionally guided by the x-ray crystal structure of the TPP1 OB-fold, mutations were made to delineate the role of each peptide in TPP1 function. The first two peptides (L_{23} and L_{45}) localized to two separate loops within the OB-fold structure (Figure 2). The L_{23} loop is a short turn connecting β2 and β3 of the OB-fold in human TPP1 and is completely conserved in mammalian sequences. In *S. cerevisiae* Cdc13, the analogous L_{23} loop forms part of the DNA-binding interface and provides an induced fit mechanism for recognition of telomere DNA (59,60). In human TPP1, the L_{23} loop is located near S111, which is phosphorylated to regulate telomerase activity (61), as well as the TEL patch, a glutamate and leucine-rich moiety critical for telomerase recruitment (49,62). To further elucidate the molecular role of the L_{23} loop in TPP1 function, the four residues that comprise this loop (^{148}DGTH) were mutated to alanine residues.

The L_{45} loop connects the β4 and β5 strands of the human TPP1 OB-fold (Figure 2). While not as conserved as the L_{23} loop, the L_{45} loop maintains a substantial degree of primary sequence homology, particularly among mammals (Figure 2A). The L_{45} loop of *S. nova* TEBPβ plays a direct role in telomere ssDNA binding, as F106 forms hydrophobic and base-stacking interactions with the ssDNA substrate in the TEBPα–TEPBβ–ssDNA complex structure (38). Other OB-fold containing proteins, including *S. nova* TEBPα and human POT1 and RPA large subunit (Rpa70), form a cleft between the L_{45} and L_{12} loops that cradles the ssDNA substrate (63). To determine what role the TPP1 L_{45} peptide plays in regulating crucial interactions with POT1, ssDNA and/or telomerase, the entire loop (192-201) was truncated and replaced with five alanine residues. This truncation/mutation was intended to alter both the chemical composition of the L_{45} loop while simultaneously limiting any putative non-specific contributions (e.g. amide backbone interactions) that the longer, native loop might solicit. Wild-type TPP1 and all TPP1 mutations were expressed and purified to homogeneity, and the structural integrity of all constructs was verified by circular dichroism spectroscopy (Supplementary Figure S4).

The peptide bearing the αC helix (^{226}QDLDVQKKLYDCL) also showed significant variations between TPP1 and POT1–TPP1 states in our H/DX

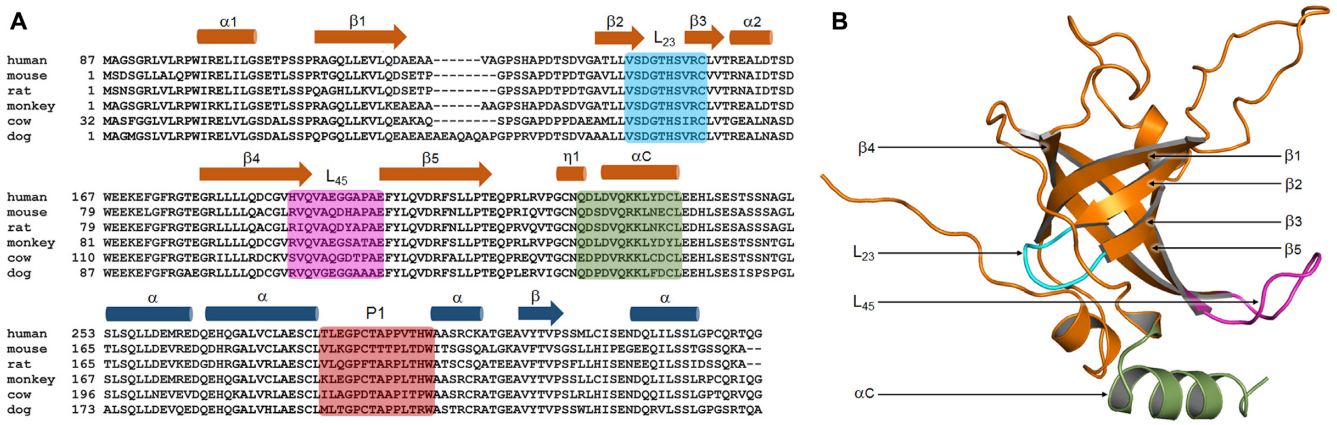

Figure 2. Locations of identified peptides within the OB-fold of TPP1. (**A**) Multiple sequence alignment comparing the primary sequence of human TPP1 with its orthologs (mouse, rat, monkey, cow and dog). Alignment was performed with Clustal-omega (71) and further formatted with Espript (72) to highlight sequence similarities and identities among the proteins. Secondary structural elements (as denoted in PDB id:2I46, chain A; α-helices as orange cylinders and β-strands as orange arrows) of human TPP1 (87–250) and peptides of interest (L_{23} in cyan, L_{45} in magenta and αC in green) are depicted over the sequence alignment. The JPred 4 (73) predicted secondary structural elements (α-helices as blue cylinders and β-strands as blue arrows) and the P1 peptide (maroon) are also depicted over the POT1-binding region. (**B**) Structure of the human TPP1 OB-fold domain. Peptide segments identified in H/DX experiments are highlighted, with the same color codes described in panel (A).

experiments. The structure of the TPP1 OB-fold domain includes the αC helix, which resides at the C-terminal end of the domain and is highly conserved across species (Figure 2). A structural comparison between the human TPP1 OB-fold with that of the orthologous *S. nova* TEBPβ protein, in the context of the TEBPα-TEBPβ-ssDNA ternary complex, reveals that this helix adopted different confirmations in the two structures (23). Although this rearrangement could be due to differences in the telomere-binding properties of different species, our H/DX data support a conformational change in the αC helix of TPP1 that occurs upon POT1-binding. The putative re-orientation of this helix to accommodate POT1 binding is discussed in more detail below.

L_{23} loop mutations impair POT1–TPP1 heterodimer formation

Several point mutations in the TPP1 binding domain of POT1 have been shown to result in a decreased recruitment of POT1 to the telomere (17). Similarly, *Tpp1* knock-down experiments cause cellular phenotypes that are similar to *Pot1* knock-down in mouse cells (26). These data indicate that TPP1 is necessary for POT1 association at the telomere and that the ssDNA-binding properties of POT1 alone do not suffice for telomere localization. While it is clear that the POT1–TPP1 interaction is important for proper telomere protection, the molecular details of this interaction have never been measured directly.

We developed a quantitative pull-down assay to determine the relative affinities between POT1 and TPP1 proteins. Here, quantification of the POT1–TPP1 interaction was determined with GST-tagged POT1 and His-tagged TPP1. Fusion proteins were individually expressed and purified and a fixed concentration of GST-tagged POT1 (10 nM) was then incubated with increasing concentrations of His-tagged-TPP1 (4 nM to 1 μM). After GST pull-down, Western blotting and densitometry was used to determine the relative abundance of GST-POT1 and His-TPP1 (Figure 3A and B). After immunoblots were quantified and plotted, the Hill Plot equation was used to calculate the relative affinities of POT1 and TPP1 in terms of their apparent equilibrium dissociation constants (K_{app}; Figure 3B). While the K_{app} calculated in this way is most certainly a gross underestimate for the true POT1–TPP1 dissociation constant, the approach provides an effective method for analyzing relative protein–protein affinities. Under these conditions, the K_{app} for POT1 and TPP1-WT was determined to be 106.9 ± 35.6 nM (Figure 3B). In these experiments, GST protein alone served as a negative control and did not bind to His-TPP1, thereby negating the possibility of non-specific interactions. These data establish the pull-down assay as a viable method to investigate and compare the relative binding of POT1 with TPP1 mutants.

To compare the relative binding contributions of the L_{23} and L_{45} peptide mutations in TPP1, we fixed the concentration of TPP1 proteins to 500 nM and quantified the normalized efficiencies for binding of the mutant proteins to GST–POT1 as compared to wild-type TPP1 (Figure 3C and D). The TPP1-L_{45} mutation displayed only a marginal reduction in GST–POT1 affinity (74.0 ± 7.8%) when compared to the wild-type TPP1 affinity for GST–POT1 under identical conditions. However, the TPP1-L_{23} mutant bound GST–POT1 only 17.5 ± 3.1% as efficiently as did wild-type TPP1 under identical conditions (Figure 3). We further analyzed the individual contributions of POT1-binding by separately mutating the four amino acids that comprise the L_{23} loop and performing additional pull-down experiments. These data indicate that point mutations to any one of the four residues within the TPP1 L_{23} loop adversely affected POT1-binding, with the D148A mutation exhibiting the most pronounced effect (Supplementary Figure S5).

It was unexpected that a peptide located outside of the well-characterized POT1-binding domain of TPP1 had such profound effects on protein–protein interactions. Thus, we next compared how this mutation compared to

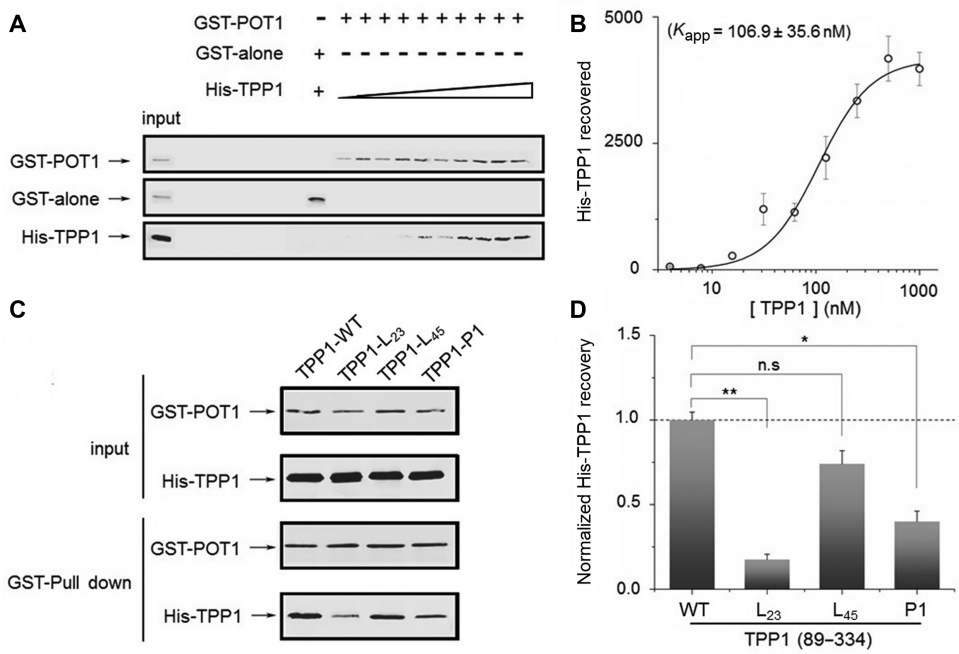

Figure 3. TPP1-L_{23} and P1 mutations impair POT1 binding capability. (**A**) Quantitative pull-down assays were used to determine the binding affinity between native POT1 and TPP1 proteins. Increasing concentrations (∼4 nM to 1 μM) of His-tagged-TPP1 were incubated with GST or GST-POT1 (10 nM). After GST-POT1 pull-down, immunoblots were used to determine the binding efficiency of His-TPP1. (**B**) The POT1-TPP1 binding affinity was calculated by plotting the relative abundance of GST–POT1 bound His-TPP1 protein as a function of increasing TPP1 concentrations. The data were then fitted by the Hill equation, which resulted in a K_{app} value of 106.9 ± 35.6 nM for the native POT1–TPP1 complex. (**C**) GST-POT1 was then used for pull-downs of TPP1-WT, TPP1-L_{23}, TPP1-L_{45} and TPP1-P1 mutants. After GST pull-down, immunoblots were used to quantitate the amount of His-TPP1 relative to GST-POT1. (**D**) The relative binding efficiencies of His-TPP1-WT and mutant variants to GST-POT1 protein were quantified from the immunoblot intensities. All values were normalized to TPP1-WT and Tukey's multiple comparison test was used to calculate TPP1–WT binding to GST–POT1. Statistical significance is reported as: n.s. = not significant, ($P > 0.05$); * = $0.05 > P > 0.001$; and ** = $P \leq 0.001$.

those within the defined PBD of TPP1. Examination of the POT1-binding domain of TPP1 from our H/DX results highlighted a peptide (^{280}TLEGPCTAPPVTHW) in the TPP1 PBD that showed differences in H/DX when comparing TPP1 with the POT1–TPP1 complex (Figure 1). This peptide, labeled P1 as it resides in the known POT1-binding domain, displayed a decrease in H/DX upon POT1-binding that was reduced from 40% to 20% (Figure 1, Supplementary Figure S3) suggesting that this region of TPP1 becomes protected from solvent exposure upon interactions with POT1. In a recent study, the corresponding P1 peptide was entirely deleted, which disrupted POT1–TPP1 interactions in mouse cells (34). We reasoned that the deletion of this entire peptide could adversely affect protein folding to disrupt POT1–TPP1 interactions by altering the secondary structure of the POT1-binding domain. To avoid this possibility, we then engineered a human–mouse chimeric protein.

Because human POT1 protein does not interact with mouse Tpp1 protein, and vice versa (26,64), we designed a chimeric human TPP1 protein that has six amino acid substitutions within the P1 peptide such that the entire 14 amino acid P1 region corresponds to the mouse Tpp1 sequence. We then performed pull-down assays to quantitate the binding efficiency between the chimeric TPP1 protein and GST–POT1. This TPP1–P1 mutation displayed impaired binding to GST–POT1 protein that was 40.0 ± 6.2% when compared to wild-type TPP1 (Figure 3). While these data indicate that the P1 peptide is a major contributor to POT1–TPP1 interactions, our data also reveal that the L_{23} mutation, which resides within the OB-fold of TPP1 has an even more pronounced effect on POT1–TPP1 interactions.

Mutations in the TPP1-L_{23} and L_{45} loops impair DNA binding of the POT1–TPP1 complex

We next employed filter-binding assays to determine whether the TPP1 mutations affected ssDNA-binding affinity of the POT1–TPP1 complex. For this assay, d(GGTTAG)$_2$ DNA (hT12wt) was used as a substrate as it contains the minimal recognition site for an individual POT1 or POT1–TPP1 protein (16,48,65). The binding affinities (K_D) of POT1 and POT1–TPP1–WT were determined to be 38.2 ± 4.8 nM and 3.8 ± 0.5 nM, respectively. These values for equilibrium binding affinities are comparable to those previously reported, and demonstrate that the inclusion of native TPP1 increases the binding affinity over POT1 alone by an order of magnitude (Figure 4) (18,23,49). The POT1–TPP1–L_{23} mutant complex resulted in a significantly reduced affinity for ssDNA (K_D = 27.3 ± 4.2 nM). Since the L_{23} mutation had such profound effects on POT1 interactions, it is not surprising that the affinity for ssDNA for the POT1–TPP1–L_{23} complex was comparable to that determined for POT1 alone. The L_{45} mutation also resulted in decreased ssDNA binding for the POT1–TPP1–L_{45} complex (K_D = 13.7 ± 5.5 nM; Figure 4). In contrast to the L_{23} mutation, the L_{45} mutation did not significantly reduce POT1–TPP1 interactions. These data indicate that the L_{45}

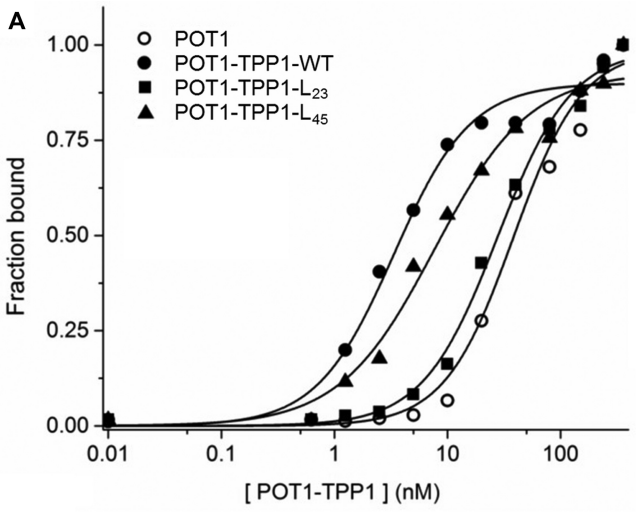

B

	K_D (nM)
POT1	38.2 ± 4.8
POT1-TPP1-WT	3.8 ± 0.5
POT1-TPP1-L_{23}	27.6 ± 4.3
POT1-TPP1-L_{45}	13.7 ± 5.5

Figure 4. The TPP1 L_{23} and L_{45} loops contribute to ssDNA binding affinity. (**A**) The dissociation constants (K_D) of POT1–TPP1 proteins and ssDNA (hT12) binding were determined under steady-state equilibrium conditions with a filter-binding assay. K_D values were calculated by plotting the fraction of protein-bound versus free DNA as a function of increasing protein concentrations (○ – POT1-alone; ●-POT1-TPP1-WT; ■-POT1-TPP1-L_{23}; ▲-POT1-TPP1-L_{45}). Data were then fit by using the Hill equation. (**B**) K_D values for individual POT1–TPP1 complexes reveal that the L_{23} mutation decreased the affinity of the complex for hT12 ssDNA nearly 10-fold, which is similar to that of POT1 alone. The L_{45} mutation slightly decreased the affinity of the POT1–TPP1 complex for hT12 DNA. All experiments were carried out in triplicate with respective errors included.

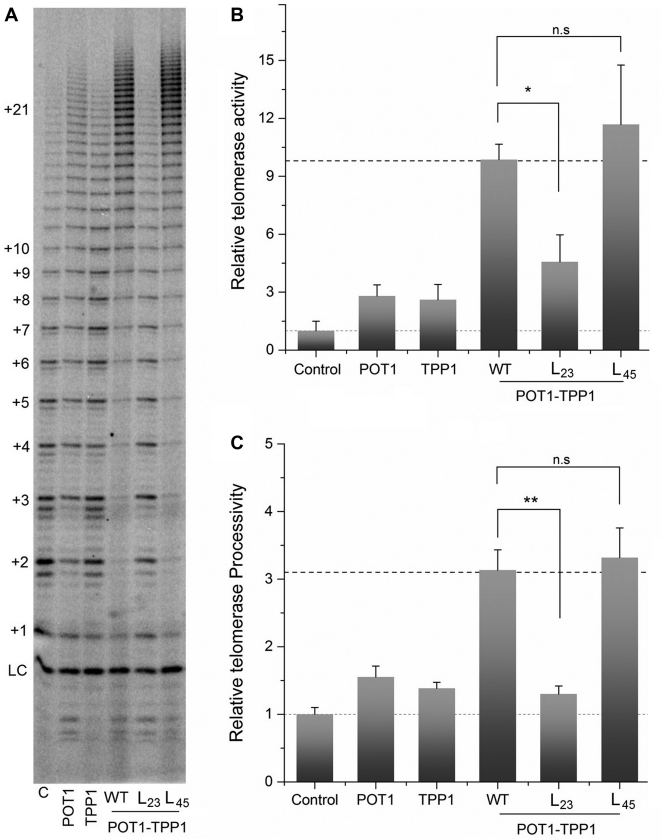

Figure 5. The TPP1 L_{23} loop is essential for POT1–TPP1 to function as a telomerase processivity enhancement factor. (**A**) This direct telomerase extension assay demonstrates enhancement of telomerase activity and processivity by the POT1–TPP1–WT heterodimer. Similar to the wild-type protein, the L_{45} mutation of TPP1 when coupled with POT1, maintained an ability to enhance telomerase activity and processivity. The L_{23} mutant, however, abrogated this POT1–TPP1–mediated enhancement. (**B**) Quantitation of total telomerase activity relative to control samples for POT1–TPP1–WT, POT1–TPP1–L_{23} and POT1–TPP1–L_{45} mutations. (**C**) Quantitation of telomerase repeat addition processivity relative to control samples for POT1–TPP1–WT, POT1–TPP1–L_{23} and POT1–TPP1–L_{45}. In panels (B) and (C), Tukey's multiple comparison test was used to calculate the statistical significance for mutant POT1–TPP1 compared to POT1–TPP1–WT. Statistical significance is reported as: n.s. = not significant, ($P > 0.05$); * = $0.05 > P > 0.001$; and ** = $P \leq 0.001$.

loop enhances the interaction of the human POT1–TPP1 heterodimer with ssDNA, possibly through direct interactions as is the case for the analogous L_{45} loop of *S. nova* TEBPβ in the TEBPα–TEBPβ–ssDNA complex (38).

The TPP1–L_{23} mutation abrogates the POT1–TPP1 enhanced stimulation of telomerase activity and processivity

Given that distinct areas of TPP1 such as the TEL patch mediate telomerase recruitment (49,62), we reasoned that regions identified in the H/DX experiments might also contribute to enhanced telomerase activity and processivity. To this end, we performed a direct primer-extension assay with human telomerase obtained from HEK293 cells after co-transfection with human TERT and TR plasmids (66). Since this enhanced telomerase activity and processivity requires both POT1 and TPP1 (18,23,29), the inclusion of either protein alone yielded only a minor increase in telomerase activity and processivity (Figure 5). As expected, inclusion of POT1–TPP1–WT significantly enhanced telomerase activity (∼10-fold) and processivity (∼3-fold) over telomerase alone. Wild-type POT1 protein was then pre-incubated with each of the TPP1 mutants (POT1–TPP1–L_{23} and POT1–TPP1–L_{45}) and then subjected to a telomerase extension assay. After 30 min, the extended ssDNA products were analyzed and the relative telomerase activity and processivity were quantified (Figure 5). Here, inclusion of POT1–TPP1–L_{23} had virtually no effect on telomerase activity or processivity when compared to POT1 protein alone. In contrast, the POT1–TPP1–L_{45} mutation enhanced telomerase activity and processivity to a degree comparable to that exhibited by POT1–TPP1–WT protein.

Together, our data show that the L_{45} loop of TPP1 is important for enhanced binding of the POT1–TPP1 complex to ssDNA, but it does not affect the ability of the POT1–TPP1 heterodimer to activate telomerase-mediated extension. This is an important separation-of-function finding that complements the opposing role described for the

TEL patch, which abrogates telomerase-mediated extension without affecting ssDNA binding events (49). Results focusing on the TPP1-L_{23} loop reveal that mutations to this region adversely affect telomerase activation. The inability of the POT1–TPP1–L_{23} complex to stimulate telomerase activity could at least in part be attributed to abrogation of POT1–TPP1 interactions caused by this mutation. The significantly reduced ability of TPP1-L_{23} to interact with POT1 would prevent the localization of TPP1-bound telomerase with POT1-bound ssDNA. In contrast, although the affinity of the POT1–TPP1–L_{45} heterodimer for ssDNA is less than that of wild-type protein, the conserved interaction between POT1 and TPP1 suffices for telomerase recruitment and stimulation. Therefore, we can conclude that the TPP1–L_{45} loop does not adversely affect telomerase recruitment to POT1, at least under our experimental conditions.

A putative rearrangement of TPP1 peptides to accommodate POT1–TPP1 heterodimer formation

Although structural information of TPP1 is limited to only its OB-fold domain, the POT1–TPP1 heterodimer is functionally analogous to the telomere-end binding (TEBPα–TEBPβ–ssDNA) complex in the ciliate, *Sterkiella nova*. A comparison between the TPP1 OB-fold with that of its *S. nova* TEBPβ counterpart revealed that the human POT1-TPP1 and *S. nova* TEBPα-TEBPβ complexes are structurally conserved even though their sequence identity is poor (18,23). A similar comparison found that the POT1–DNA binding domain is structurally analogous to that of TEBPα (16) (Supplementary Figure S6). These data indicate that telomere complexes that recognize telomere ssDNA overhangs are structurally conserved and that the human POT1–TPP1 complex is very likely to assemble as a tertiary structure that is similar to the *S. nova* TEBPα–TEBPβ–ssDNA complex, which has been solved by x-ray crystallography (38).

To gain insight into potential conformational changes of those TPP1 peptides that arise upon POT1- and/or ssDNA-binding, we analyzed the structure of the human OB-fold of apo-TPP1 along with that of *S. nova* TEBPβ in complex with TEBPα and ssDNA (Figure 6A). As expected, the β-barrel of the two structures superposed with variations between the two structures residing primarily in the peripheral loops that connect β-strands within the OB-fold. The orientation of the peripheral L_{45} loop is different in the two structures, and analysis of the B-factors further implicates the inherent flexibility of this particular loop in the apo-TPP1 protein (Figure 6B). In addition to the L_{45} loop, the other region of apo-TPP1 with the highest B-factor values corresponded to the αC helix, which displays an increased H/D exchange in response to POT1-binding. Interestingly, the αC helix was rotated by ∼19° in the TEBPα–TEBPβ–ssDNA complex compared to that of TPP1 alone (Figure 6A). Furthermore, these two regions with high B-factors in the OB-fold of apo-TPP1 revealed surprisingly low B-factor values in the TEBPα–TEBPβ–ssDNA complex (Figure 6B). In the absence of a POT1–TPP1 structure, or that of TEBPα–TEBPβ without ssDNA, it is impossible to identify structural changes due to protein–protein interactions versus ssDNA binding. However, the structural comparison combined with the H/DX and functional data presented here are consistent with a model in which POT1-binding results in a structural rearrangement of the αC helix of TPP1 and ssDNA binding stabilizes the L_{45} peptide of TPP1 within the POT1–TPP1–ssDNA complex (Figure 6C and D).

DISCUSSION

Our biophysical and biochemical data highlight critical regions of TPP1 that are involved in dynamic functions of this versatile telomere protein. The peptide fragment containing the L_{23} loop showed minimal deuteration for TPP1 and POT1-TPP1 proteins, but drastically enhanced accessibility to D_2O solvent exchange in the POT1-TPP1-ssDNA ternary complex. This finding indicates that the L_{23} fragment becomes more solvent accessible, perhaps due to a structural rearrangement, upon DNA binding to the POT1-TPP1 heterodimer. Interestingly, the L_{23} loop is localized on the OB-fold domain of TPP1 in an area that is crucial for TPP1 function, primarily in a 'hotspot' region that regulates interactions with telomerase. For example, previous studies have shown that a D148A point mutation, which resides within the L_{23} loop, disrupts TPP1-telomerase interactions (61). Also, S111 is located in an area that is immediately adjacent to the L_{23} loop (Figure 7). S111 can be phosphorylated, which is important for regulating telomerase recruitment and activity in a cell cycle dependent manner (61). In addition, the TEL patch is localized to a region that is immediately proximal to the L_{23} loop. However, unlike S111 and the TEL patch, our data demonstrate that mutations to the L_{23} loop equally abrogate POT1-binding interactions.

Homology modeling, using the *S. nova* TEBPα–TEBPβ–ssDNA complex as a guide, places the L_{23} loop of TPP1 in an area predicted to come into direct contact with POT1 when the two proteins form a heterodimer (Figure 6C). Our pull-down experiments confirm this role, and are supported by other findings as well. For example, mutations to the analogous and highly conserved L_{23} loop in *Candida albicans* ever shorter telomeres 3 (Est3) protein results in loss of telomere maintenance (67). In the structure of the TPP1 OB-fold, the L_{23} loop of TPP1 coordinates water-mediated, intramolecular hydrogen bonding interactions (Figure 7). Interestingly, the H-bonding network of the TPP1 L_{23} involves the C-terminal αC helix. Our data demonstrate that the C-terminal αC helix becomes more susceptible to H/DX after POT1-binding. These interactions are preserved in the structures of other telomere end-binding proteins, including *S. cerevisiae* Est3 (37), suggesting a common structure-function relationship across species.

Our studies additionally identified the L_{45} loop as a peptide that exhibits environmental changes upon ternary complex formation. Notably, the deuterium exchange of the L_{45} peptide did not change upon binding to the POT1 protein, but was significantly diminished upon binding of the POT1–TPP1 heterodimer to telomere ssDNA. Mutations to the L_{45} loop resulted in diminished ssDNA-binding of the POT1–TPP1 heterodimer. In the *S. nova* TEBPα–TEBPβ–ssDNA structure, the analogous L_{45} loop (R99-

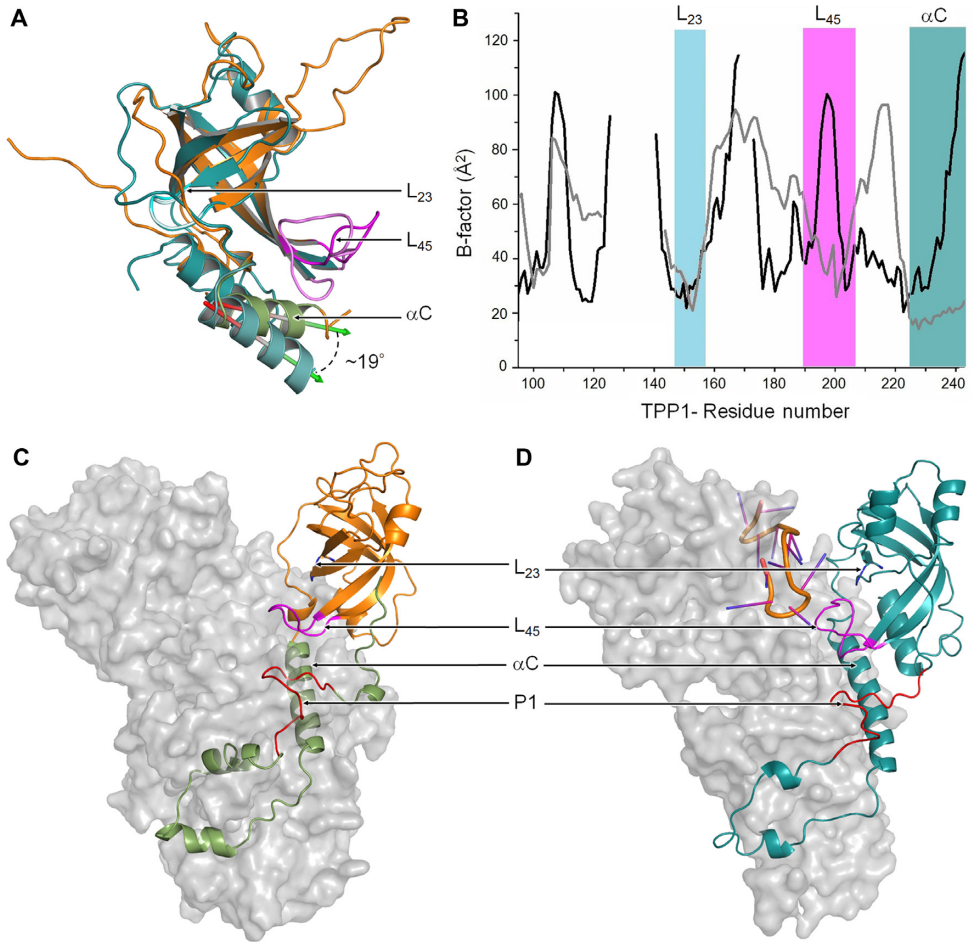

Figure 6. Conformational flexibility of critical peptide segments and their structural variations in TPP1 and *S. nova* TEBPβ OB-fold domains. (**A**) A structural comparison of the OB-fold domain of human TPP1 from the apo structure with that of *S. nova* TEBPβ in the TEBPα–TEBPβ–ssDNA ternary complex. The superimposition shows that the L_{23} loop adopts identical conformations in the two structures, whereas the L_{45} loop displays variations in peptide and relative arrangements. The αC helix displays angular variations as well, which may reflect a conformational rearrangement due to POT1/TEBPα and/or ssDNA binding. (**B**) B-factor analysis of the peptide-backbone (Cα) of free TPP1 and TEBPα in the TEBPα–TEBPβ–ssDNA complex indicates that the L_{45} and αC peptide segments are more flexible in free TPP1 than in the TEBPα–TEBPβ–ssDNA ternary complex. (**C**) The predicted model of the human POT1–TPP1 complex. The POT1 homology model is shown as a grey isosurface, the TPP1-OB-fold domain is in orange, and the predicted TPP1–PBD is in green. The POT1–TPP1 complex was modeled with the *S. nova* TEBPα–TEPBβ–ssDNA structure as a template. L_{23}, L_{45}, αC and P1 segments are labeled. (**D**) Crystal structure of the *S. nova* TEBPα–TEPBβ heterodimer, where TEBPα is shown as a grey isosurface and TEBPβ as a teal cartoon model. The bound ssDNA substrate is shown as an orange backbone.

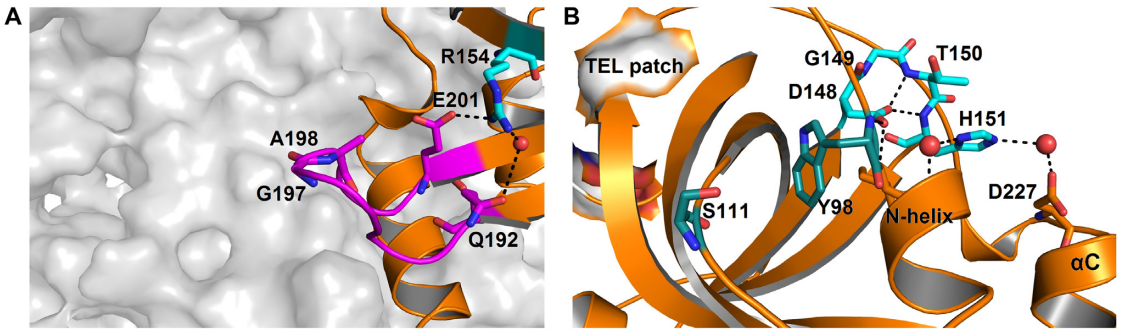

Figure 7. Structural and functional implications of the L_{23} and L_{45} peptides. (**A**) The L_{45}-loop (magenta) of human TPP1 extends away from the core OB-fold and toward the putative ssDNA-binding pocket. A salt bridge formed between R154, Q192 and E201 supports the extended orientation of the TPP1 L_{45}-loop. (**B**) The L_{23} loop (shown in cyan) in human TPP1 forms a hydrogen-bonding network within the core of the OB-fold domain that connects the L_{23} loop with the αC-helix.

L112) is in a structurally conserved position similar to that of human TPP1 and directly interacts with telomeric DNA (dG10) through the S102-A103 backbone (38). Additionally, F106, also within the orthologous L_{45} loop of TEBPβ, provides base stacking interactions with dG9 of ssDNA. Despite low sequence identity within the L_{45} loop of TPP1 and TEBPβ, the lower deuteration of the TPP1 L_{45} peptide fragment in the POT1–TPP1–ssDNA ternary complex compared to that of POT1–TPP1 protein alone suggests that this loop plays a conserved structural role in stabilizing interactions between the protein and DNA.

A recent study identified a mutation in the TPP1 gene that is associated with cutaneous malignant melanoma and prostate cancer in humans (68). This mutation results in an A200T point mutation at the protein level that corresponds to a residue within the L_{45} loop. Based on our data, it is likely that this particular point mutation alters the recognition or the affinity of the POT1–TPP1 complex for telomere DNA, resulting in genomic instability. This interaction unlikely is unique to the TPP1 protein as there are multiple proteins with OB-fold domains that use the analogous L_{45} loops to coordinate DNA interactions. In human POT1, the structural analog of the L_{45} loop in the first OB-fold domain includes amino acids that are critical for binding to telomere DNA (Supplementary Figure S7). In this loop, the Y89 base stacks with dG4 of the ssDNA (16). Interestingly, a POT1 Y89C mutation is a rare variant that has been identified in patients suffering from familial melanoma (69). Similarly, the analogous L_{45} loop of the human RPA 70 subunit maintains a functional role in ssDNA recognition and binding (Supplementary Figure S7). F386 of RPA70 and dC18 of the bound DNA substrate are responsible for coordinating this interaction (70). In contrast to the prior examples, yeast Est3 contains a significantly longer L_{45}-like peptide that adopts a highly structured helical conformation (Supplementary Figure S7). This loop appears to be dispensable to Est3 function, as its deletion does not impair cell viability or alter telomere length (37). Together, these findings provide insights into how nucleic acid binding proteins might utilize a conserved OB-fold protein for binding, while the loops have diverged to fulfill specialized functions.

Finally, our investigations focused on the P1 peptide, within the POT1-binding domain of TPP1, provide additional insight for this peptide's role in POT1–TPP1 complex formation. Although alterations in the sequence of this peptide decreased its binding affinity with POT1, such mutations were insufficient to entirely disrupt protein–protein interactions. These observations indicate that other peptides within TPP1 are also involved in POT1-TPP1 interactions. Since alternate peptides were not identified within the POT1-binding domain in our H/DX study, it is possible that a series of interactions that are individually undetectable by H/DX collectively contribute to protein–protein interactions. Another possible explanation is that regions outside of the known POT1-binding domain provide more significant contributions to POT1–TPP1 interactions. Indeed, our data reveal that mutations to the L_{23} loop drastically affected POT1-binding events.

Without question, structural biology provides an essential means for identifying functional motifs and comparing analogous structures. But additional biophysical techniques, such as H/DX coupled with MS, are very informative when analyzing conformational changes that are important for protein function and for characterizing protein–protein and protein–nucleic acid interfaces within complexes that are not amenable to structural investigation. Our study uniquely focuses on addressing the nature of such conformational states in human TPP1 as it undergoes structural rearrangements upon POT1- and ssDNA-binding. Combined with mutagenesis, our results indicate that the peripheral loops of the TPP1 OB-fold are functionally dynamic whereas the β-barrel undergoes few changes upon complex formation. These findings help to explain how multiple proteins use a conserved fold for nucleic acid binding, while the loops connecting β-strands within that fold could make an underappreciated contribution toward substrate specificity and regulation of diverse functions.

SUPPLEMENTARY DATA

Supplementary Data are available at NAR Online.

ACKNOWLEDGEMENTS

This work was supported by grants from the National Institutes of Health (DP2 CA186571) and the American Cancer Society (RSG-13-211-01-DMC) to D.J.T. and the Arnold and Mabel Beckman Foundation to K.P. K.P. is the John H. Hord Professor of Pharmacology at Case Western Reserve University, Cleveland, Ohio, USA.

FUNDING

National Institutes of Health (NIH) [DP2 CA186571 to D.J.T.]; American Cancer Society [RSG-13-211-01-DMC to D.J.T.]; Arnold and Mabel Beckman Foundation [to K.P.]. Funding for open access charge: National Institutes of Health (NIH) [DP2 CA186571].
Conflict of interest statement. None declared.

REFERENCES

1. Blackburn,E.H. (1991) Structure and function of telomeres. *Nature*, **350**, 569–573.
2. Guo,X., Deng,Y., Lin,Y., Cosme-Blanco,W., Chan,S., He,H., Yuan,G., Brown,E.J. and Chang,S. (2007) Dysfunctional telomeres activate an ATM-ATR-dependent DNA damage response to suppress tumorigenesis. *EMBO J.*, **26**, 4709–4719.
3. Denchi,E.L. and de Lange,T. (2007) Protection of telomeres through independent control of ATM and ATR by TRF2 and POT1. *Nature*, **448**, 1068–1071.
4. Blackburn,E.H. (1994) Telomeres: no end in sight. *Cell*, **77**, 621–623.
5. Huffman,K.E., Levene,S.D., Tesmer,V.M., Shay,J.W. and Wright,W.E. (2000) Telomere shortening is proportional to the size of the G-rich telomeric 3′-overhang. *J. Biol. Chem.*, **275**, 19719–19722.
6. Wright,W.E., Tesmer,V.M., Huffman,K.E., Levene,S.D. and Shay,J.W. (1997) Normal human chromosomes have long G-rich telomeric overhangs at one end. *Genes Dev.*, **11**, 2801–2809.
7. de Lange,T. (2005) Shelterin: The protein complex that shapes and safeguards human telomeres. *Genes Dev.*, **19**, 2100–2110.
8. Bianchi,A., Smith,S., Chong,L., Elias,P. and de Lange,T. (1997) TRF1 is a dimer and bends telomeric DNA. *EMBO J.*, **16**, 1785–1794.
9. Smogorzewska,A., van Steensel,B., Bianchi,A., Oelmann,S., Schaefer,M.R., Schnapp,G. and de Lange,T. (2000) Control of human telomere length by TRF1 and TRF2. *Mol. Cell. Biol.*, **20**, 1659–1668.

10. Baumann,P. and Cech,T.R. (2001) Pot1, the putative telomere end-binding protein in fission yeast and humans. *Science*, **292**, 1171–1175.
11. Li,B., Oestreich,S. and de Lange,T. (2000) Identification of human Rap1: Implications for telomere evolution. *Cell*, **101**, 471–483.
12. O'Connor,M.S., Safari,A., Liu,D., Qin,J. and Songyang,Z. (2004) The human Rap1 protein complex and modulation of telomere length. *J. Biol. Chem.*, **279**, 28585–28591.
13. Kim,S.H., Kaminker,P. and Campisi,J. (1999) TIN2, a new regulator of telomere length in human cells. *Nat. Genet.*, **23**, 405–412.
14. Ye,J.Z., Hockemeyer,D., Krutchinsky,A.N., Loayza,D., Hooper,S.M., Chait,B.T. and de Lange,T. (2004) POT1-interacting protein PIP1: a telomere length regulator that recruits POT1 to the TIN2/TRF1 complex. *Genes Dev.*, **18**, 1649–1654.
15. Houghtaling,B.R., Cuttonaro,L., Chang,W. and Smith,S. (2004) A dynamic molecular link between the telomere length regulator TRF1 and the chromosome end protector TRF2. *Curr. Biol.*, **14**, 1621–1631.
16. Lei,M., Podell,E.R. and Cech,T.R. (2004) Structure of human POT1 bound to telomeric single-stranded DNA provides a model for chromosome end-protection. *Nat. Struct. Mol. Biol.*, **11**, 1223–1229.
17. Liu,D., Safari,A., O'Connor,M.S., Chan,D.W., Laegeler,A., Qin,J. and Songyang,Z. (2004) PTOP interacts with POT1 and regulates its localization to telomeres. *Nat. Cell Biol.*, **6**, 673–680.
18. Xin,H., Liu,D., Wan,M., Safari,A., Kim,H., Sun,W., O'Connor,M.S. and Songyang,Z. (2007) TPP1 is a homologue of ciliate TEBP-beta and interacts with POT1 to recruit telomerase. *Nature*, **445**, 559–562.
19. Palm,W. and de Lange,T. (2008) How shelterin protects mammalian telomeres. *Annu. Rev. Genet.*, **42**, 301–334.
20. Blackburn,E.H. (2005) Telomeres and telomerase: Their mechanisms of action and the effects of altering their functions. *FEBS Lett.*, **579**, 859–862.
21. Greider,C.W. and Blackburn,E.H. (1985) Identification of a specific telomere terminal transferase activity in Tetrahymena extracts. *Cell*, **43**, 405–413.
22. Hockemeyer,D. and Collins,K. (2015) Control of telomerase action at human telomeres. *Nat. Struct. Mol. Biol.*, **22**, 848–852.
23. Wang,F., Podell,E.R., Zaug,A.J., Yang,Y., Baciu,P., Cech,T.R. and Lei,M. (2007) The POT1-TPP1 telomere complex is a telomerase processivity factor. *Nature*, **445**, 506–510.
24. O'Connor,M.S., Safari,A., Xin,H., Liu,D. and Songyang,Z. (2006) A critical role for TPP1 and TIN2 interaction in high-order telomeric complex assembly. *Proc. Natl. Acad. Sci. U.S.A.*, **103**, 11874–11879.
25. Liu,D., O'Connor,M.S., Qin,J. and Songyang,Z. (2004) Telosome, a mammalian telomere-associated complex formed by multiple telomeric proteins. *J. Biol. Chem.*, **279**, 51338–51342.
26. Hockemeyer,D., Palm,W., Else,T., Daniels,J.P., Takai,K.K., Ye,J.Z., Keegan,C.E., de Lange,T. and Hammer,G.D. (2007) Telomere protection by mammalian Pot1 requires interaction with Tpp1. *Nat. Struct. Mol. Biol.*, **14**, 754–761.
27. Nandakumar,J., Podell,E.R. and Cech,T.R. (2010) How telomeric protein POT1 avoids RNA to achieve specificity for single-stranded DNA. *Proc. Natl. Acad. Sci. U.S.A.*, **107**, 651–656.
28. Abreu,E., Aritonovska,E., Reichenbach,P., Cristofari,G., Culp,B., Terns,R.M., Lingner,J. and Terns,M.P. (2010) TIN2-tethered TPP1 recruits human telomerase to telomeres in vivo. *Mol. Cell. Biol.*, **30**, 2971–2982.
29. Latrick,C.M. and Cech,T.R. (2010) POT1-TPP1 enhances telomerase processivity by slowing primer dissociation and aiding translocation. *EMBO J.*, **29**, 924–933.
30. Ray,S., Bandaria,J.N., Qureshi,M.H., Yildiz,A. and Balci,H. (2014) G-quadruplex formation in telomeres enhances POT1/TPP1 protection against RPA binding. *Proc. Natl. Acad. Sci. U.S.A.*, **111**, 2990–2995.
31. Hwang,H., Buncher,N., Opresko,P.L. and Myong,S. (2012) POT1-TPP1 regulates telomeric overhang structural dynamics. *Structure*, **20**, 1872–1880.
32. Mullins,M.R., Rajavel,M., Hernandez-Sanchez,W., de la Fuente,M., Biendarra,S.M., Harris,M.E. and Taylor,D.J. (2016) POT1-TPP1 binding and unfolding of telomere DNA discriminates against structural polymorphism. *J. Mol. Biol.*,**428**, 2695–2708.
33. Kibe,T., Osawa,G.A., Keegan,C.E. and de Lange,T. (2010) Telomere protection by TPP1 is mediated by POT1a and POT1b. *Mol. Cell. Biol.*, **30**, 1059–1066.
34. Kibe,T., Zimmermann,M. and de Lange,T. (2016) TPP1 Blocks an ATR-Mediated Resection Mechanism at Telomeres. *Mol. Cell*, **61**, 236–246.
35. Bochkareva,E., Kaustov,L., Ayed,A., Yi,G.S., Lu,Y., Pineda-Lucena,A., Liao,J.C., Okorokov,A.L., Milner,J., Arrowsmith,C.H. *et al.* (2005) Single-stranded DNA mimicry in the p53 transactivation domain interaction with replication protein A. *Proc. Natl. Acad. Sci. U.S.A.*, **102**, 15412–15417.
36. Bryan,C., Rice,C., Harkisheimer,M., Schultz,D.C. and Skordalakes,E. (2013) Structure of the human telomeric Stn1-Ten1 capping complex. *PloS One*, **8**, e66756.
37. Rao,T., Lubin,J.W., Armstrong,G.S., Tucey,T.M., Lundblad,V. and Wuttke,D.S. (2014) Structure of Est3 reveals a bimodal surface with differential roles in telomere replication. *Proc. Natl. Acad. Sci. U.S.A.*, **111**, 214–218.
38. Horvath,M.P., Schweiker,V.L., Bevilacqua,J.M., Ruggles,J.A. and Schultz,S.C. (1998) Crystal structure of the Oxytricha nova telomere end binding protein complexed with single strand DNA. *Cell*, **95**, 963–974.
39. Yang,H., Jeffrey,P.D., Miller,J., Kinnucan,E., Sun,Y., Thoma,N.H., Zheng,N., Chen,P.L., Lee,W.H. and Pavletich,N.P. (2002) BRCA2 function in DNA binding and recombination from a BRCA2-DSS1-ssDNA structure. *Science*, **297**, 1837–1848.
40. Rajavel,M., Mullins,M.R. and Taylor,D.J. (2014) Multiple facets of TPP1 in telomere maintenance. *Biochim. et Biophys. Acta*, **1844**, 1550–1559.
41. Murzin,A.G. (1993) OB(oligonucleotide/oligosaccharide binding)-fold: common structural and functional solution for non-homologous sequences. *EMBO J.*, **12**, 861–867.
42. Theobald,D.L., Mitton-Fry,R.M. and Wuttke,D.S. (2003) Nucleic acid recognition by OB-fold proteins. *Annu. Rev. Biophys. Biomol. Struct.*, **32**, 115–133.
43. Zhang,Z. and Smith,D.L. (1993) Determination of amide hydrogen exchange by mass spectrometry: A new tool for protein structure elucidation. *Protein Sci.*, **2**, 522–531.
44. Engen,J.R. (2009) Analysis of protein conformation and dynamics by hydrogen/deuterium exchange MS. *Anal. Chem.*, **81**, 7870–7875.
45. Orban,T., Jastrzebska,B., Gupta,S., Wang,B., Miyagi,M., Chance,M.R. and Palczewski,K. (2012) Conformational dynamics of activation for the pentameric complex of dimeric G protein-coupled receptor and heterotrimeric G protein. *Structure*, **20**, 826–840.
46. Mandell,J.G., Falick,A.M. and Komives,E.A. (1998) Measurement of amide hydrogen exchange by MALDI-TOF mass spectrometry. *Anal. Chem.*, **70**, 3987–3995.
47. Taylor,D.J., Podell,E.R., Taatjes,D.J. and Cech,T.R. (2011) Multiple POT1-TPP1 proteins coat and compact long telomeric single-stranded DNA. *J. Mol. Biol.*, **410**, 10–17.
48. Corriveau,M., Mullins,M.R., Baus,D., Harris,M.E. and Taylor,D.J. (2013) Coordinated interactions of multiple POT1-TPP1 proteins with telomere DNA. *J. Biol. Chem.*, **288**, 16361–16370.
49. Nandakumar,J., Bell,C.F., Weidenfeld,I., Zaug,A.J., Leinwand,L.A. and Cech,T.R. (2012) The TEL patch of telomere protein TPP1 mediates telomerase recruitment and processivity. *Nature*, **492**, 285–289.
50. Orban,T., Bereta,G., Miyagi,M., Wang,B., Chance,M.R., Sousa,M.C. and Palczewski,K. (2010) Conformational changes in guanylate cyclase-activating protein 1 induced by Ca2+ and N-terminal fatty acid acylation. *Structure*, **18**, 116–126.
51. Orban,T., Huang,C.C., Homan,K.T., Jastrzebska,B., Tesmer,J.J. and Palczewski,K. (2012) Substrate-induced changes in the dynamics of rhodopsin kinase (G protein-coupled receptor kinase 1). *Biochemistry*, **51**, 3404–3411.
52. Tsybovsky,Y., Orban,T., Molday,R.S., Taylor,D. and Palczewski,K. (2013) Molecular organization and ATP-induced conformational changes of ABCA4, the photoreceptor-specific ABC transporter. *Structure*, **21**, 854–860.
53. Xu,H. and Freitas,M.A. (2007) A mass accuracy sensitive probability based scoring algorithm for database searching of tandem mass spectrometry data. *BMC Bioinformatics*, **8**, 133–142.
54. Xu,H. and Freitas,M.A. (2008) Monte carlo simulation-based algorithms for analysis of shotgun proteomic data. *J. Proteome Res.*, **7**, 2605–2615.

55. Weis,D.D., Engen,J.R. and Kass,I.J. (2006) Semi-automated data processing of hydrogen exchange mass spectra using HX-Express. *J. Am. Soc. Mass Spectrom.*, **17**, 1700–1703.
56. Zaug,A.J., Podell,E.R., Nandakumar,J. and Cech,T.R. (2010) Functional interaction between telomere protein TPP1 and telomerase. *Genes Dev.*, **24**, 613–622.
57. Zaug,A.J., Crary,S.M., Jesse Fioravanti,M., Campbell,K. and Cech,T.R. (2013) Many disease-associated variants of hTERT retain high telomerase enzymatic activity. *Nucleic Acids Res.*, **41**, 8969–8978.
58. Xu,H. and Freitas,M.A. (2009) MassMatrix: a database search program for rapid characterization of proteins and peptides from tandem mass spectrometry data. *Proteomics*, **9**, 1548–1555.
59. Eldridge,A.M. and Wuttke,D.S. (2008) Probing the mechanism of recognition of ssDNA by the Cdc13-DBD. *Nucleic Acids Res.*, **36**, 1624–1633.
60. Mitton-Fry,R.M., Anderson,E.M., Theobald,D.L., Glustrom,L.W. and Wuttke,D.S. (2004) Structural basis for telomeric single-stranded DNA recognition by yeast Cdc13. *J. Mol. Biol.*, **338**, 241–255.
61. Zhang,Y., Chen,L.Y., Han,X., Xie,W., Kim,H., Yang,D., Liu,D. and Songyang,Z. (2013) Phosphorylation of TPP1 regulates cell cycle-dependent telomerase recruitment. *Proc. Natl. Acad. Sci. U.S.A.*, **110**, 5457–5462.
62. Sexton,A.N., Youmans,D.T. and Collins,K. (2012) Specificity requirements for human telomere protein interaction with telomerase holoenzyme. *J. Biol. Chem.*, **287**, 34455–34464.
63. Horvath,M.P. (2011) Structural anatomy of telomere OB proteins. *Crit. Rev. Biochem. Mol. Biol.*, **46**, 409–435.
64. Palm,W., Hockemeyer,D., Kibe,T. and de Lange,T. (2009) Functional dissection of human and mouse POT1 proteins. *Mol. Cell. Biol.*, **29**, 471–482.
65. Loayza,D., Parsons,H., Donigian,J., Hoke,K. and de Lange,T. (2004) DNA binding features of human POT1: A nonamer 5′-TAGGGTTAG-3′ minimal binding site, sequence specificity, and internal binding to multimeric sites. *J. Biol. Chem.*, **279**, 13241–13248.
66. Cristofari,G. and Lingner,J. (2006) Telomere length homeostasis requires that telomerase levels are limiting. *EMBO J.*, **25**, 565–574.
67. Yu,E.Y., Wang,F., Lei,M. and Lue,N.F. (2008) A proposed OB-fold with a protein-interaction surface in Candida albicans telomerase protein Est3. *Nat. Struct. Mol. Biol.*, **15**, 985–989.
68. Aoude,L.G., Pritchard,A.L., Robles-Espinoza,C.D., Wadt,K., Harland,M., Choi,J., Gartside,M., Quesada,V., Johansson,P., Palmer,J.M. *et al.* (2015) Nonsense mutations in the shelterin complex genes ACD and TERF2IP in familial melanoma. *J. Natl. Cancer Inst.*, **107**, 1–7.
69. Robles-Espinoza,C.D., Harland,M., Ramsay,A.J., Aoude,L.G., Quesada,V., Ding,Z., Pooley,K.A., Pritchard,A.L., Tiffen,J.C., Petljak,M. *et al.* (2014) POT1 loss-of-function variants predispose to familial melanoma. *Nat. Genet.*, **46**, 478–481.
70. Bochkarev,A., Pfuetzner,R.A., Edwards,A.M. and Frappier,L. (1997) Structure of the single-stranded-DNA-binding domain of replication protein A bound to DNA. *Nature*, **385**, 176–181.
71. Sievers,F., Wilm,A., Dineen,D., Gibson,T.J., Karplus,K., Li,W., Lopez,R., McWilliam,H., Remmert,M., Soding,J. *et al.* (2011) Fast, scalable generation of high-quality protein multiple sequence alignments using Clustal Omega. *Mol. Syst. Biol.*, **7**, 539.
72. Robert,X. and Gouet,P. (2014) Deciphering key features in protein structures with the new ENDscript server. *Nucleic Acids Res.*, **42**, W320–W324.
73. Drozdetskiy,A., Cole,C., Procter,J. and Barton,G.J. (2015) JPred4: A protein secondary structure prediction server. *Nucleic Acids Res.*, **43**, W389–W394.